Plasma Sources Sci. Technol. **19** (2010) 015008 (11pp) doi:10.1088/0963-0252/19/1/015008

Capacitively coupled plasma used to simulate Titan's atmospheric chemistry

G Alcouffe[1], M Cavarroc[2], G Cernogora[1], F Ouni[1], A Jolly[3], L Boufendi[4] and C Szopa[5]

[1] Université de Versailles St Quentin, LATMOS BP3 - 91371 Verrières-le-Buisson Cedex France
[2] MID Dreux Innovation, 4 rue Albert Caquot, 28500 Vernouillet, France
[3] LISA, Université Paris 12, 61 avenue du Général de Gaulle, 94010 Créteil Cédex, France
[4] GREMI Université d'Orléans BP6744 - 45067 Orléans Cedex2 France
[5] UPMC, Univ Paris 06, LATMOS BP3-91371 Verrières-le-Buisson Cedex France

E-mail: gregoire.alcouffe@latmos.ipsl.fr

Received 15 May 2009, in final form 18 May 2009
Published 10 November 2009
Online at stacks.iop.org/PSST/19/015008

Abstract
A complex chemistry in Titan's atmosphere leads to the formation of organic solid aerosols. We use a radio-frequency (RF) capacitively coupled plasma discharge produced in different N_2–CH_4 mixtures (from 0% to 10% of CH_4) to simulate this chemistry. The work presented here was devoted to the study of the plasma discharge. In our experiment, the electron density is measured by the resonant cavity method and is about 10^{15} m^{-3} in pure N_2 plasma at 30 W excitation RF power. It decreases by a factor of 2 as soon as CH_4 is present in the discharge, even for a proportion as small as 2% of CH_4. An optical emission spectroscopy diagnostic is installed on the experiment to study the evolution of the N_2 bands and to perform actinometry measurements using Ar lines. This diagnostic allowed us to measure variations in the electron temperature and to show that a decrease in the density of the electrons can be compensated by an increase in their energy. We have also used an experimental setup where the plasma is tuned in a pulsed mode, in order to study the formation of dust particles. We observed variations in the self-bias voltage, the RF injected power and the intensities of the nitrogen bands, which indicated that dust particles were formed. The characteristic dust formation time varied, depending on the experimental conditions, from 4 to 110 s. It was faster for higher pressures and for smaller proportions of CH_4 in the gas mixture.

(Some figures in this article are in colour only in the electronic version)

1. Introduction

Among the solar system bodies of interest, Titan, the biggest satellite of Saturn, presents a structure similar to Earth, i.e. a solid surface and a dense atmosphere composed of N_2 and CH_4. In this atmosphere, solid aerosols are produced in large amounts, covering Titan with an orange veil. The descent of the European Huygens probe into Titan's atmosphere in 2005 enabled the collection of more data on these aerosols than ever. Among these data, very interesting ones were produced by the descent imager/spectral radiometer (DISR) and aerosol collector and pyrolyser (ACP) experiments. By comparing scattered light measurements by DISR with numerical simulations of the optical depth of the atmosphere, it has been shown that aerosols are aggregates of grains about 0.1 μm in diameter (Tomasko *et al* 2005). ACP experiment, designed to analyse *in situ* the chemical composition of the aerosols, showed that the main pyrolysis products were HCN and NH_3. These components are fingerprints, indicating that tholins include a solid organic refractory core, made of carbon and nitrogen (Israel *et al* 2005).

To understand the formation of these solid particles, many laboratory experiments have been devoted to the production of analogues of Titan's aerosols, named tholins. The most efficient processes for tholins production are plasma discharges: spark discharges (De Vanssay *et al* 1995), dielectric barrier discharges (Majumdar *et al* 2005), corona discharges (Gonzalez *et al* 2001, Ramirez *et al* 2005), radio frequency

 © 2010 IOP Publishing Ltd Printed in the UK

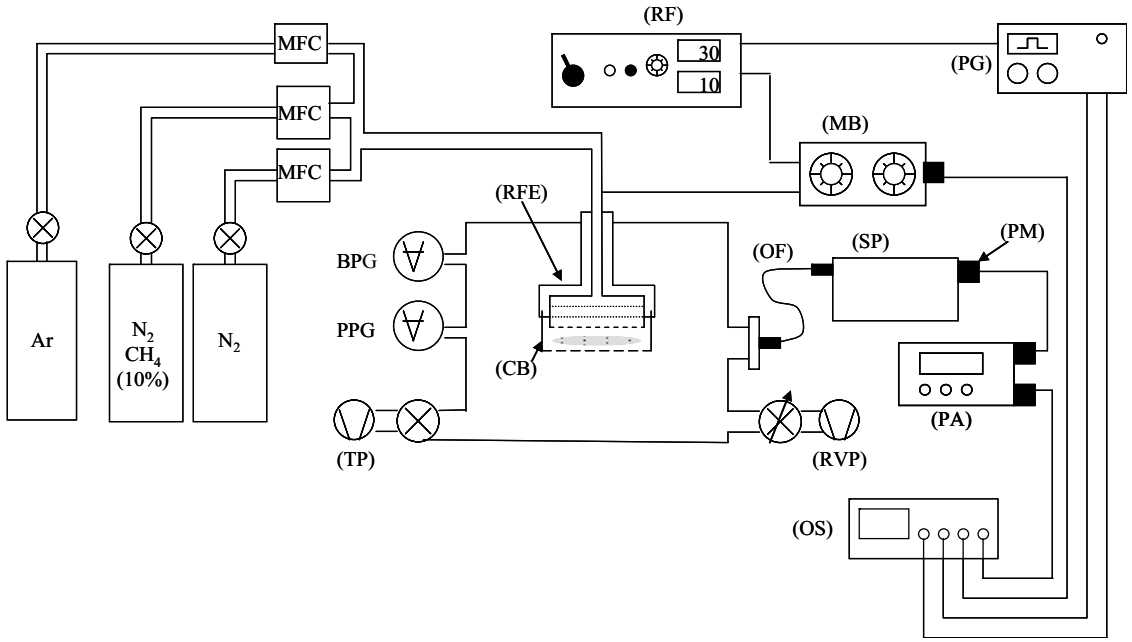


Figure 1. Experimental setup of the PAMPRE experiment. MFC—mass flow controllers; BPG—capacitance pressure gauge; CPG—penning pressure gauge; TP—turbomolecular pump; RFE—RF electrode; CB—confining box; RF—RF generator; PG—pulse generator; MB—match box; OS—oscilloscope; OF—optical fiber; SP—UV–VIS–NIR Monochromator; PM—photomultiplier; PA—picoammeter; RVP—rotary vane pump.

inductively coupled plasma (ICP) discharges (Imanaka *et al* 2004) or direct current (DC) discharges (Coll *et al* 1999, Bernard *et al* 2003). In all these devices, though tholins are produced as a thin layer deposited on solid surfaces, which may have an influence on their formation chemistry.

In the work presented here, we used a capacitively coupled plasma (CCP) discharge in order to avoid any surface interactions during the tholins production. This kind of plasma is well known to produce dust particles in suspension in the gas phase. While they grow, the particles produced are charged and experience a set of forces which keep them in levitation: electrostatic force, thermophoresis force, their weight, the neutral drag force and the ion drag force (Spears *et al* 1986, 1988, Watanabe 1988, Selwyn *et al* 1989, Bouchoule and Boufendi 1993, Bouchoule 1999). The combination of these forces defines their equilibrium and trapping in the gas phase of the plasma. The particles are kept in levitation between the electrodes until their weight and the resulting gravitational force are too strong and they are expelled from the discharge. Many studies have been and are still being done to understand their formation and growth mechanisms. These studies have shown that dust particles are formed by aggregation of nanocrystalline structures 2–3 nm in diameter (Boufendi *et al* 1994, Cavarroc 2006).

Dusty plasmas are also used to reproduce astrophysical dusty environments, such as cometary tails, planetary environments or interplanetary dust clouds (Draine 1987). For example, studies have been performed in hydrocarbon-based (C_2H_2) plasmas (Kovacevic *et al* 2003, Hong *et al* 2003) to study interstellar dust.

The goal of the work presented here was to study the properties of a CCP RF discharge produced from a N_2–CH_4 mixture and simulating Titan's atmosphere. The experiment is named PAMPRE, a French acronym for Production d'Aérosols en Microgravité par Plasma Reactif (Szopa *et al* 2006).

2. Experimental setup

The experimental setup is presented in figure 1. The reaction chamber is a stainless-steel cylinder 30 cm in diameter and 40 cm in height. The plasma is created and confined in a metallic box 13.7 cm in diameter and with a 4–5 cm inter-electrode gap. The bottom of the box is a grid to allow sweeping the dust out. On the side of the box, two 1 cm-wide apertures, covered with a thin grid (0.2 mm thick), allow studying the plasma using optical emission spectroscopy. This configuration, already used in the GREMI laboratory (Boufendi *et al* 1994), is in agreement with the 'GEC RF Reference cell' (Hargis *et al* 1994). In addition to the optical emission spectroscopy (OES) diagnostic, measurements from a resonant microwave cavity, an electrostatic probe and the self-bias voltage (V_{dc}) are used to study the plasma.

2.1. Plasma production

The plasma in PAMPRE is produced by an RF discharge. The RF power is provided by a 13.56 MHz generator (SAIREM GRP01KE) through a match box. The total power can be raised up to 100 W. Incident and reflected powers are measured to determine the RF power coupled to the plasma. The discharge can be operated in a continuous regime or a pulsed mode. The pulsed mode is triggered by a pulse generator at 2 mHz, with a 90 : 10 duty cycle (TTi TG 550). The plasma is then turned on during 350–450 s and switched off during 50 s. Such periods allow both a sufficiently long visualization of

the tholins formation (see below) and a complete gas renewal in the chamber, between two pulses. In the pulsed mode, the measurements of OES, V_{dc} and RF power presented in this paper were acquired on a 4-channel numerical oscilloscope (Tektronix TDS2004B).

The plasma is produced from a N_2–CH_4 gas mixture. The gas mixing ratio can be varied from 0% to 10% of CH_4 in high-purity nitrogen (>99.999%) using a bottle of premixed N_2–CH_4 gas mixture (10% CH_4, purity > 99.999%) and a bottle of high-purity nitrogen (purity > 99.999%). The amounts of gas injected from each bottle are controlled by two gas mass flow controllers (MKS 100 sccm full scale). Thanks to a third mass flow controller (MKS 10 sccm full scale), a small amount of argon (a few per cents) can be added to the gas mixture to use as an actinometer. The gas mixture is injected through a shower-type biased electrode, 12.6 cm in diameter, to provide a laminar gas flow into the plasma box. It is pumped using a rotary vane vacuum pump whose pumping speed is controlled by a throttle valve. The pressure is measured by a capacitance gauge (MKS baratron). Typically, a total flow rate of 55 sccm is used, giving a pressure, P, of 0.9 mbar. A lower pressure ($P < 0.9$ mbar) can be obtained by reducing the total gas flow rate using the mass flow controller; and a higher pressure ($P > 0.9$ mbar) can be obtained by reducing the pumping speed using the throttle valve. Before each experiment, the chamber is pumped with a turbomolecular pump. In our experimental conditions, the RF discharge can operate at a total pressure ranging from 0.2 to 10 mbar.

2.2. Optical emission spectroscopy

The light emitted by the plasma is collected through a silica window by a silica optical fibre and transmitted to a UV–VIS–NIR, 60 cm focal length, high resolution monochromator (Jobin Yvon) connected to a photomultiplier (Hamamatsu R928). The output current of the photomultiplier is measured with a picoammeter (Keithley 6485), and recorded on a PC. The use of this device constitutes a great improvement to the previous setup (Szopa *et al* 2006) and allows the observation of the N_2 bands rotational structures.

In the study presented here, spectra were recorded in the UV range (371 to 394 nm) to measure $N_2(C)$, N_2^+ and CN bands, in the steady-state conditions. The Ar line at 811.5 nm was recorded in the near IR through a coloured glass filter rejecting second order lines.

2.3. Electron and ion densities measurements

Since the dimensions of the confining box are of the order of a few centimetres, it can be used as a microwave resonant cavity. The electron density can then be inferred from the cavity's resonance mode frequency shift (Slater 1946, Papoular 1991, Donovan *et al* 1993, Dressel *et al* 1993, Klein *et al* 1993), using the following equation:

$$n_e = A 8\pi^2 f^2 \frac{\Delta f}{f_0} \frac{m_e \varepsilon_0}{e^2}, \quad (1)$$

where n_e is the electron density, f_0 is the resonance mode frequency of the empty cavity, f is the resonance mode frequency of the plasma filled cavity, $\Delta f = f - f_0$, e and m_e are the electron charge and mass, respectively, and A is a geometrical factor which depends on the electric field and the electron density spatial distributions. The factor A was calculated by Haverlag *et al* (1991), on a similar RF discharge (GEC reference cell configuration) to be between 1 and 1.8. In our case, we assume $A = 1$, such that equation (1) gives a mean value of n_e.

To excite and detect the resonance modes of the cavity, two loop antennas electrically isolated from the discharge box are symmetrically placed in the plasma box, on the bottom grid, 3 cm away from its axis. One is the emitter, connected to a microwave signal generator (Rhode and Schwarz), the other one is the receiver, connected to a Schottky diode, itself connected to a numerical oscilloscope. The resolution of the resulting frequency measurements is 1 MHz. Three resonance modes have been detected in the cavity without plasma: TM_{010}, TM_{110} and TM_{210}. As the TM_{210} mode (3579 MHz) is the most intense mode, it is the one we use to measure the resonance frequency shift and infer the plasma electron density.

In addition, the plasma ion density is measured using a plane stainless-steel Langmuir probe, 5 mm in diameter. This probe is placed 3 cm away from the axis, the bottom of the cage, and is electrically isolated from it. It is biased using a dc generator. The potential V is measured with a high impedance voltmeter (1 GΩ). As the probe is not compensated for RF conditions, only the ion part of its characteristic $I(V)$ is recorded. The ion density is deduced from the ion saturation current I_{is} which is expressed as

$$I_i = 0.6 n_i q_i S \sqrt{\frac{k_B T_e}{m_i}}, \quad (2)$$

where n_i is the ion density, q_i is the ion charge, k_B is Boltzmann's constant, T_e is the electron temperature, m_i is the ion mass and S is the surface of the probe (Allen *et al* 1995). As T_e cannot be deduced from the electron part of the Langmuir probe's characteristic, we assume $T_e \approx 2$ eV in our ion density calculation.

2.4. Self-bias voltage V_{dc}

A self-bias voltage (Bogaerts *et al* 2002) appears at the driven electrode of a radio frequency CCP discharge if both electrodes differ in size, and when a blocking capacitor (here inside the match box) is inserted between the RF generator and the electrode (or when the electrode is non-conductive). The self-bias (V_{dc}) variation is related to the electron density and the electron temperature. It has already been shown that the appearance of dust in the discharge induces perturbations of V_{dc} (Praburam and Goree 1996, Samsonov and Goree 1999). These perturbations are explained by the fact that, during their growth, the solid particles attach some of the electrons present in the plasma. It results in a decrease in electron density, and a variation of V_{dc}. V_{dc} then stabilizes to a constant value (Mikikian and Boufendi 2004, Cavarroc 2006).

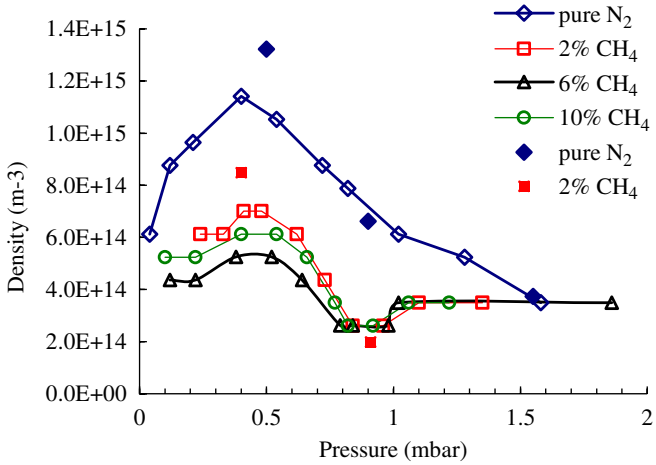


Figure 2. Electron and ion densities as a function of pressure in pure N_2 and in N_2–CH_4 plasmas. The hollow symbols represent the electron density measurements obtained from the cavity's resonance mode. The full symbols represent the ion density measurements obtained with the Langmuir probe.

3. Results and discussion (plasma in steady-state conditions)

3.1. Electron and ion densities

In the study presented here, we have measured the electron and ion densities in plasmas produced with 30 W injected RF power, for different pressure conditions and gas mixtures, as shown in figure 2.

We can see that, in a pure N_2 plasma, the electron density increases with pressure from 0.1 to 0.4 mbar, reaches a maximum at 0.4 mbar ($n_e = 1.2 \times 10^{15}\,m^{-3}$) and then decreases. In N_2–CH_4 plasmas, the electron density variations with pressure, for different proportions of CH_4 in the mixture (2%, 6% and 10%), are similar to the ones in pure N_2. However, the electron density maximum, around 0.4 mbar, is strongly reduced compared with that for pure N_2, even for a proportion of CH_4 as low as 2% ($n_e = 7 \times 10^{14}\,m^{-3}$). In addition, in N_2–CH_4 plasmas, the electron density reaches a minimum at a pressure of 0.8–0.9 mbar and seems to remain constant and independent of the amount of CH_4 in the gas mixture for pressures above 1 mbar. The uncertainty on the electron density minimum is high because the measured Δf is close to 1 MHz, which is the frequency resolution of the measurement. For a similar reason, measurements at $P > 1$ mbar only show a tendency.

In a pure N_2 plasma, the ion density, n_i, deduced from the Langmuir probe measurements at 0.5, 0.9 and 1.55 mbar is close to the electron density, n_e. This is coherent with the electrical quasi-neutrality property of the plasma. In N_2–CH_4 plasmas, a solid insulating film is deposited on the probe surface such that the probe has to be cleaned after each measurement. Consequently, only a few probe characteristics have been recorded. Figure 2 shows the ion density measurements obtained in a plasma with 2% of CH_4 in the gas mixture, for two different pressures: 0.4 and 0.9 mbar. Here again, the Langmuir probe gives a value of positive ion density almost equal to the electron density.

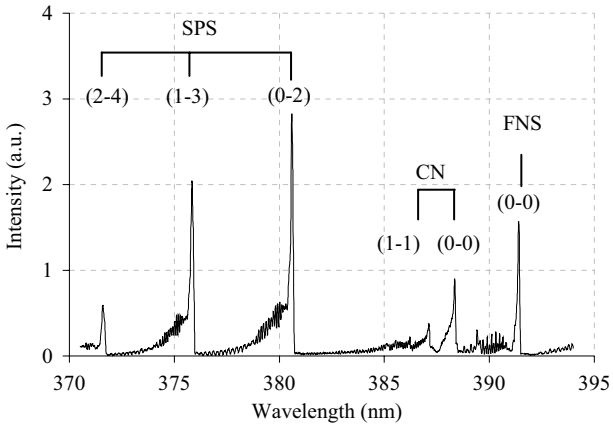


Figure 3. UV spectrum of a N_2–CH_4 plasma in the 370–395 nm range (2% CH_4, 1 mbar).

Then, no difference between ion and electron density can be detected with the used Langmuir probe setup. Then, up to now, the density of negative ions cannot be measured. However, the observed decay in n_e between pure N_2 and N_2–CH_4 mixture is confirmed, and is interpreted as electron attachment on dust particles.

3.2. OES measurements

In the UV spectra we recorded in N_2–CH_4 plasmas, several of the bands observed have been identified. Figure 3 shows the UV spectrum of a plasma produced in a N_2–CH_4 gas mixture with 2% CH_4. The bands at 370 nm , 375.5 nm and 380.5 nm correspond, respectively, to the (2–4), (1–3) and (0–2) transitions of the N_2 second positive system (SPS), emitted from the $N_2(C)$ level; the band at 391.4 nm corresponds to the (0–0) transition of the N_2 first negative system (FNS), emitted from the $N_2^+(B)$ level and the bands at 387.3 nm and 388.3 nm correspond, respectively, to the (1–1) and (0–0) transitions of the CN violet system, emitted from the CN(B) level. For the latter, a little contribution from the (1–1) transition, emitted from N_2^+ at 388.4 nm, is possible (Pearse and Gaydon 1976).

3.2.1. Neutral gas temperature. The rotational structure of the SPS N_2 bands is relatively well resolved. By fitting the experimental spectra with spectra calculated by models that take into account the rotational temperature and the instrumental apparatus function, it is then possible to deduce the N_2 rotational temperature, which is equal to the neutral gas temperature T_{NG} in our experimental conditions. In our study, in order to get the best signal to noise ratio and infer a more precise N_2 rotational temperature, we fitted the experimental spectra of the most intense SPS band (i.e. the (0–0) transition at 337.1 nm). Figure 4 presents an example of fit. For that experimental spectrum, a gas temperature of 405 K was deduced.

To check the accuracy and the validity of this method, we have studied the rotational temperature variations with injected RF power. The results are presented in figure 5. As expected, the temperature increases with RF power. Below 30 W

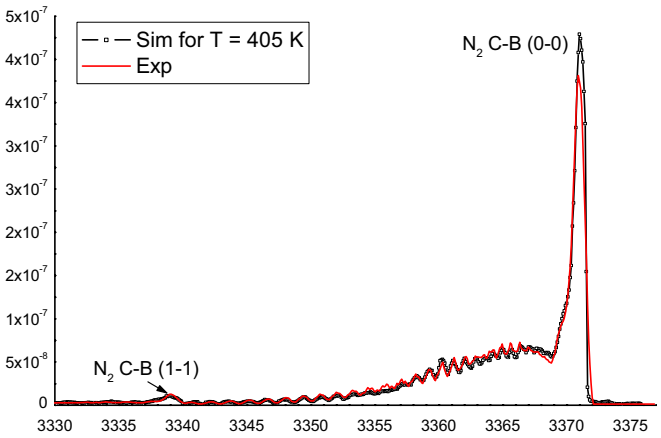


Figure 4. Measured (full curve) and calculated (curve and empty squares) rotational spectrum of the (0–0) SPS band of N_2.

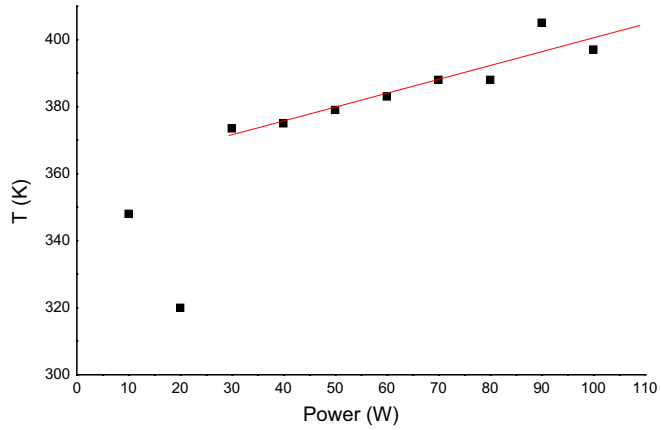


Figure 5. Variations of T_{NG} with RF power for a pressure of 0.9 mbar and a gas mixture with 2% of CH_4

RF power, the rotational line intensities are weak, inducing great uncertainties on the comparison between calculated and recorded spectra. A linear variation of temperature with RF power from 30 to 100 W is observed. The gas heating is weak, even for a power of 100 W. This is explained by the fact that, in our configuration, the plasma volume is 7.4×10^2 cm^3, which leads to a maximum injected power of 0.14 W cm^{-2}. Moreover, since the plasma diameter is high, the current density is low, which limits the gas heating as well.

For a given injected RF power, we have observed that the gas temperature increases when the pressure increases, in agreement with the increase in the electron–neutral collision frequency.

We have also studied the evolution of the neutral gas temperature as a function of the proportion of CH_4 in the gas mixture for a given pressure, as shown in figure 6. In our working conditions, the gas temperature decreases when the amount of CH_4 increases. This effect is not well understood. As mentioned before, when CH_4 is injected in the plasma, the electron density, n_e, is strongly reduced compared with the electron density in a pure nitrogen plasma. However, in a N_2–CH_4 plasma, the variations of n_e with the amount of CH_4 injected are small. In our study, in the conditions where the neutral gas temperature was measured, the electron density

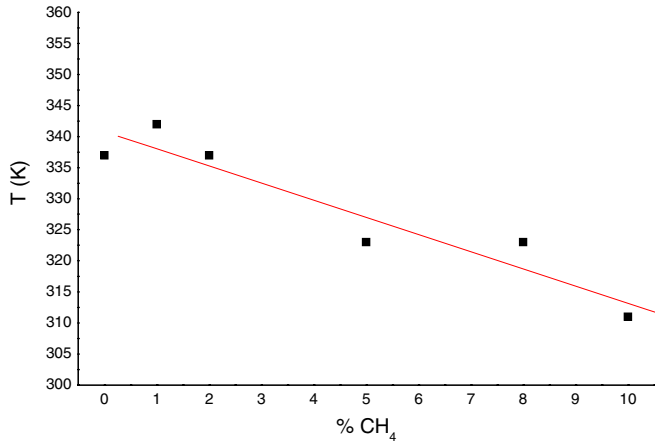


Figure 6. Variations of T_{NG} with the amount of CH_4 in the gas mixture, for a total pressure of 0.9 mbar and an RF power of 30 W.

was below the sensitivity of the electron density measurements such that we could not follow its evolution. The observed decrease in the gas temperature could then be due to the decay in electron density. This hypothesis must be validated with plasma modelling.

Note that in figures 5 and 6, the inferred temperatures vary only a little for similar conditions. Thus, in a N_2–CH_4 plasma with 2% CH_4 at 0.9 mbar, when changing the RF power, we obtained a temperature of about 370 K for an absorbed RF power of 30 W as shown in figure 5; whereas when changing the amount of CH_4 in the N_2–CH_4 gas mixture of a plasma produced at 0.9 mbar and with a 30 W RF power, we obtained a temperature of about 340 K, as shown in figure 6. This kind of variation, of about 10%, is representative of the reproducibility of our results.

3.2.2. Band and line intensities. The intensities of the N_2, N_2^+ and CN bands presented in figure 3 were measured as a function of pressure and N_2–CH_4 mixing ratio. In addition, we used the Ar lines, whose intensities were measured in the near IR range, as an actinometer. In actinometry techniques, the 750 nm Ar line is often used (see for instance Lee *et al* (1983), Jenq *et al* (1994) and Macko *et al* (2004)). However, in nitrogen discharges, some overlapping can occur with the (4–2) band of the nitrogen first positive system (FPS) at 750.4 nm (Pearse and Gaydon 1976). In our study, in order to avoid this FPS band overlapping, we chose to use the 811.5 nm Ar line for our actinometry measurements. This line is very intense, with a 3.31×10^5 s^{-1} transition probability emitted from an excited state at 13.07 eV from the Ar ground state (NIST). This excited level is then populated by electrons coming from the tail of the electron energy distribution function, i.e. in the same energy range as the $N_2(C)$ excited level ($\approx$11 eV) such that it can be used for actinometry measurements with N_2. In addition, this strong Ar line at 811.5 nm is measurable even if the coloured filter used for the measurements induces some absorption, and even if the quantum efficiency of the photomultiplier and the spectrometer grating are not optimum in the near IR range.

Figures 7(*a*) to (*d*) show the evolution of the N_2, N_2^+ and CN bands as well as the 811.5 nm Ar line as a function of

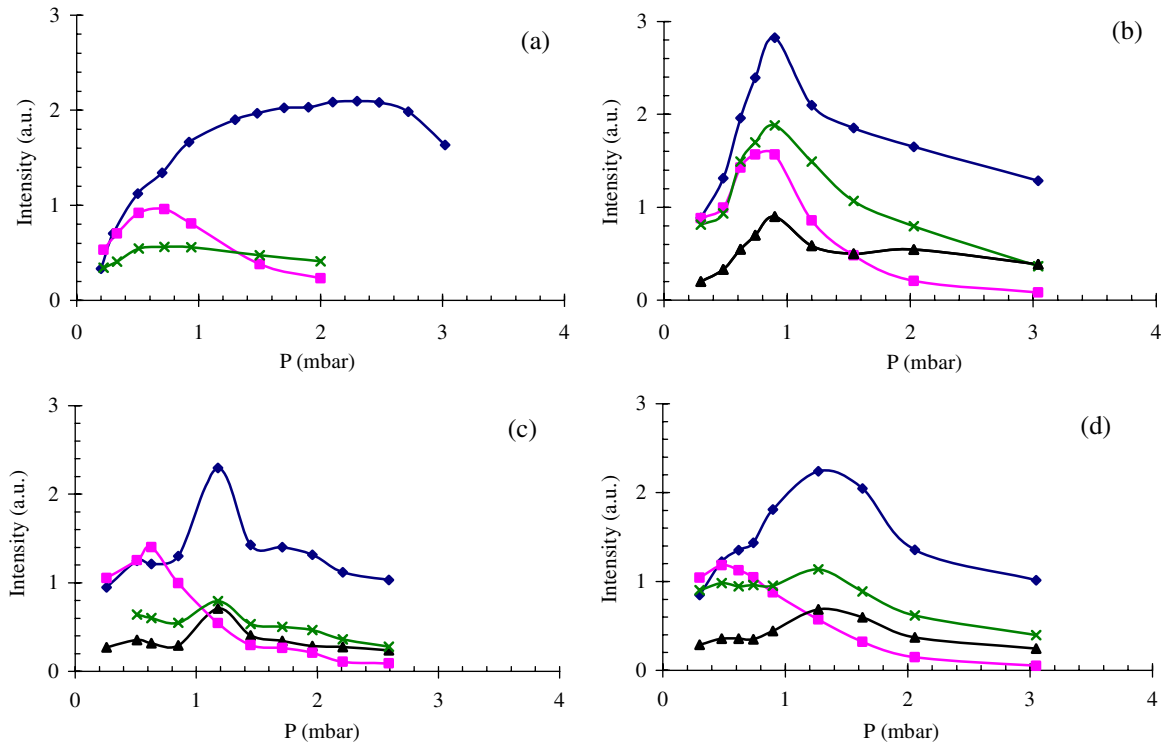


Figure 7. Intensities of the N_2, N_2^+ and CN bands and of the Ar line as a function of pressure for different proportions of CH_4 in the gas mixture: 0% (*a*), 2% (*b*), 6% (*c*) and 10% (*d*). Diamonds represent $I_{N_2(C)}$ (SPS), squares $I_{N_2^+}$ (FNS), triangles I_{CN} (CN band) and crosses I_{Ar} (Ar line).

pressure in different N_2–CH_4 gas mixtures (0%, 2%, 6% and 10% of CH_4). Since the three bands of the SPS of $N_2(C)$ present the same variations with pressure, only the most intense band, corresponding to the (0–2) transition at 380.5 nm, is presented here.

In a pure N_2 plasma (figure 7(*a*)), we observed that the N_2 (SPS) band intensity is maximal around 2.5 mbar, whereas the N_2^+ (FNS) band and the Ar line are maximal at 0.7 mbar. In N_2–CH_4 plasmas with 6% and 10% of CH_4, the intensities of the N_2 (SPS) and CN bands and of the Ar line are maximal between 1.2 and 1.5 mbar, while the N_2^+ (FNS) band is maximal at 0.5 mbar, such as the electron density. For a N_2–CH_4 plasma with 2% of CH_4, all the band intensities (including FNS) as well as the Ar line intensity are maximal at 1 mbar.

In the plasma, the Ar excited levels are populated by electron collisions,

$$e + \mathrm{Ar} \rightarrow e + \mathrm{Ar}^* \tag{3}$$

and depopulated by radiative transition only. Each Ar line intensity can then be expressed, using a coronal model, as

$$I(\mathrm{Ar}) = C\frac{n_e[\mathrm{Ar}]k_e^{\mathrm{Ar}^*}(T_e)}{A_{ij}}, \tag{4}$$

where $k_e^{\mathrm{Ar}^*}(T_e)$ is the electron excitation coefficient of the Ar excited level, A_{ij} is the Einstein coefficient for the observed line and C is a factor taking into account the spectral response of the optical setup and the volume of the observed plasma. The term $k_e^{\mathrm{Ar}^*}(T_e)$ is a representative of the evolution of the electron energy. As A_{ij} and C are constant, (4) gives

$$k_e^{\mathrm{Ar}^*}(T_e) \propto \frac{I(\mathrm{Ar})}{n_e[\mathrm{Ar}]}, \tag{5}$$

where [Ar] is the argon concentration in the gas mixture and n_e is the measured electron density (cf figure 2). The evolution of $k_e^{\mathrm{Ar}^*}(T_e)$ with pressure can then be calculated. It is presented in figure 8, in arbitrary units, for different N_2–CH_4 gas mixtures (with 0%, 2%, 6% and 10% of CH_4).

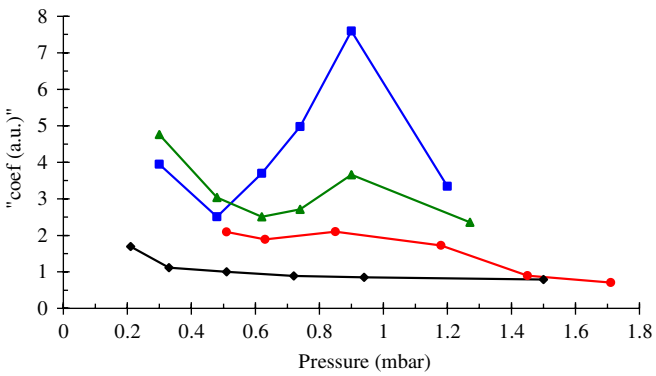


Figure 8. Evolution of $k_e^{\mathrm{Ar}^*}(T_e)$ with pressure for different proportions of CH_4: 0% (diamonds), 2% (squares), 6% (circles) and 10% (triangles).

The $k_e^{\mathrm{Ar}^*}(T_e)$ calculations at pressures from 0.9 to 1.8 mbar only show a tendency and must be taken cautiously. Indeed, as mentioned before, the large uncertainty on n_e measurements induces a large uncertainty on $k_e^{\mathrm{Ar}^*}(T_e)$ calculations.

In a pure N_2 plasma discharge, we observed that $k_e^{Ar^*}(T_e)$ decreases when the pressure increases. Such a variation is consistent with the physics of plasma discharges which predicts that the electron energy decreases when the pressure increases.

We observed that the excitation coefficient $k_e^{Ar^*}(T_e)$ is higher in N_2–CH_4 mixtures than in pure N_2 discharges. This can be explained by an increase in the electron energy in order to balance the electron density decrease due to the attachment on the dust particles and to sustain the discharge.

In N_2–CH_4 plasma discharges, for pressures ranging from 0.5 to 0.8 mbar, we observed that $k_e^{Ar^*}(T_e)$ varies with pressure. This might be due to variations in kinetics of dust formation, which could differ for different CH_4 amounts. For pressures over 1.1 mbar, the electron density can be considered constant in N_2–CH_4 mixtures (cf figure 2) and $k_e^{Ar^*}(T_e)$, deduced from (5), decreases. This result must be taken with caution and only as a tendency because, at such pressures, the density measurements are very close to their resolution limit.

If the population processes of $N_2(C)$ are also done only by electron collisions, we have

$$e + N_2(X) \rightarrow e + N_2(C). \tag{6}$$

Considering that the $N_2(C)$ energy level is ≈11 eV, i.e. in the same energy range as the Ar^* excited level, the $N_2(C)$ band and Ar line intensities should vary the same way. Figure 7(*a*) clearly shows that it is not the case in a pure N_2 plasma: their maxima are found to be at 2 mbar and 0.5 mbar, respectively. This indicates that the electron collisions alone are not sufficient to explain the population processes of the $N_2(C)$ excited state in pure N_2. The pooling reaction of $N_2(A)$ between metastable states may also contribute to populating the $N_2(C)$ excited state (Piper *et al* 1988). This reaction can be expressed as

$$N_2(A) + N_2(A) \rightarrow N_2(C) + N_2(X). \tag{7}$$

In all the N_2–CH_4 mixtures, the $N_2(C)$ band and Ar line intensities vary in the same way. This might mean that, as soon as CH_4 is present in the discharge, the population processes by electron collisions of the $N_2(C)$ excited state are dominant. This can be due to an efficient quenching of $N_2(A)$ by the CH_4 molecules (Slanger *et al* 1973):

$$N_2(A) + CH_4 \rightarrow N_2(X) + CH_4. \tag{8}$$

Thus, figures 7(*b*)–(*d*) show that in N_2–CH_4 mixtures, electronic collisions are the dominant process for the population of the $N_2(C)$ excited state.

For all conditions, figure 7 shows that the intensities of the CN band and Ar line vary the same way. This indicates that I_{CN} does not depend only on CN concentration, but also on electron processes. However, there is still a doubt on the interpretation of the results on CN as the $CN(B)$ state can be populated in different ways. Electron collisions are considered here, but other mechanisms have been observed. Iwai *et al* (1967) first proposed two chemiluminescence's population processes described in the following complementary equations:

$$N + N + XCN \rightarrow CN(B\,^2\Sigma) + N_2(X) + X \tag{9}$$

and

$$N + N + CN(X) \rightarrow CN(B\,^2\Sigma) + N_2(X), \tag{10}$$

where X may be CN or CH_3.

Then, Provencher *et al* (1971) and Washida *et al* (1975) added two other possible processes, described in equations (10) and (11):

$$N_2(A) + CN(X_2\,\Sigma^+) \rightarrow CN(B\,^2\Sigma) + N_2, \tag{11}$$

$$C + N + M \rightarrow CN(B_2\,\Sigma^+) + M, \tag{12}$$

where M is a third body.

Up to now, it has therefore been difficult for us to make a correlation between the intensity of the CN bands and the amount of CN in the discharge. It is still too early to investigate further, without a numerical simulation of the discharge.

To fully understand the OES results, all processes involved in the population of radiative excited states have to be taken into account. This must be done with a numerical model. Recent numerical calculations in pure N_2 discharges indicate that the $N_2(A)$ concentration is about $10^{12}\,m^{-3}$. This tends to show that the pooling effect probably acts significantly on the $N_2(C)$ excited level. This work is still in progress (Marques *et al* 2008a, 2008b).

4. Results and discussion for plasma in pulsed mode

In pulsed mode, the four channels of the numerical oscilloscope are used to study the transient regime. The following parameters are measured: the RF reflected, P_r, and incident, P_i, powers in the discharge; the intensity of the SPS (0–2) band at 380.4 nm measured by OES (noted I_{SPS}), and the self-bias voltage of the biased electrode V_{dc}. The plasma is thus studied by measuring its optical and electrical characteristics.

By keeping P_i constant, the variations of P_r allow measuring the effective absorbed RF power. When the absorbed RF power increases, the electric field in the discharge gets stronger. This induces an increase in electron temperature (Jouanny 2005). As already shown in section 3.2, in N_2–CH_4 mixtures, the $N_2(C)$ excited level is mainly populated by electron collisions. Thus, the intensity I_{SPS} can be deduced from an equation similar to equation (4), and depends both on the electron density and an excitation coefficient which is a function of the electron temperature. Measuring the evolution of I_{SPS} thus gives indications on the electron density and temperature evolutions. As for V_{dc}, it is connected with the electron flow impacting the electrode and mainly depends on the electron density and little on the electron temperature.

In the study presented here, the measurements were done in N_2–CH_4 plasmas with different proportions of CH_4, from 0% to 10%, and at pressures ranging from 0.7 to 1.7 mbar (in pulsed mode, the plasma gets instable below 0.7 and above 1.7 mbar). The match box was tuned to minimize the reflected power in continuous working conditions, and was not changed during the transient regime.

Figures 9 and 10 present typical oscillograms recorded in a pure N_2 plasma and in a (98% N_2–2% CH_4) plasma, respectively. In both figures, the left axis represents positive

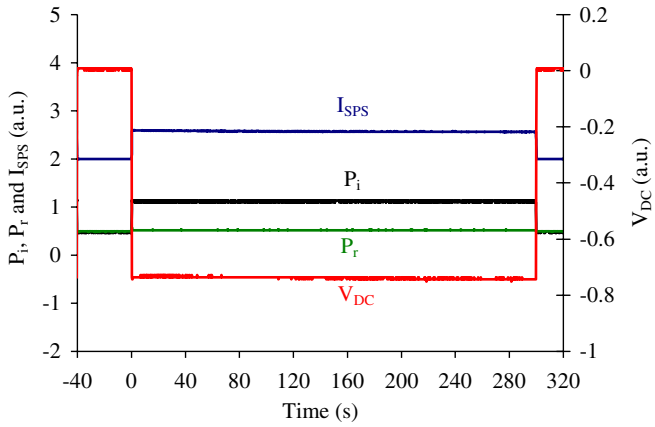


Figure 9. Oscillogram recorded in a N_2 plasma.

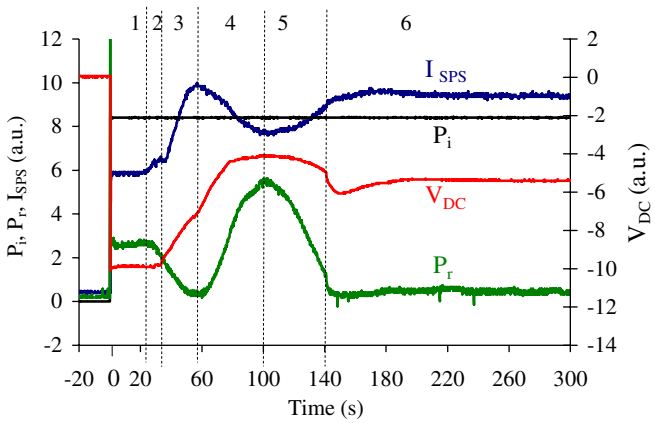


Figure 10. Oscillogram recorded in a N_2–CH_4 plasma with 2% of CH_4.

values (I_{SPS}, P_i and P_r), and the right axis negative values (V_{dc}). As V_{dc} is a negative voltage, we will consider its absolute value $|V_{dc}|$ in the future discussions to avoid confusions. Thus, a decrease in V_{dc} will mean an increase in $|V_{dc}|$ and vice versa. All the values are in arbitrary units. Moreover, the zero levels of the positive signals are shifted to allow a clear visualization and identification of each channel.

We have observed that in N_2 discharges (figure 9), V_{dc}, P_r and I_{SPS} are constant as long as the plasma is on, while in N_2–CH_4 discharges (figure 10) they vary due to the presence of dust in the discharge. I_{SPS} and P_r are strongly correlated: their variations begin at the same time, and all their extrema are reached simultaneously. On the other hand, $|V_{dc}|$ starts varying a little later, and its variations are different from those of I_{SPS} and P_r. However, it reaches its minimum value at the same time as I_{SPS} and P_r reach one of their extrema.

All variations stop at the same time when continuous working conditions (CWC) are reached. P_r is then stable at its minimal value and I_{SPS} is stable at a higher value than when the plasma was switched on. This is in agreement with the OES observations presented in the previous section, and shows that the excitation coefficient is higher in N_2–CH_4 mixtures, due to a higher electron temperature (cf figure 8). On the other hand, the $|V_{dc}|$ value in CWC is lower than at ignition, which means that the electron flow on the electrode is reduced. This confirms the results presented in figure 3 and shows that n_e decreases when CH_4 is injected in the discharge.

We can observe six phases in a N_2–CH_4 discharge, as shown in figure 10. During phase 1, the plasma is switched on, but no variations are observed. The similarity between this phase and the behaviour shown in figure 9 for a N_2 discharge leads to the conclusion that no dusts are formed yet. P_r is not minimal here: this is due to the fact that the match box is tuned to minimize P_r only in CWC. This phase lasts for a few seconds.

The beginning of phase 2 is indicated by the first observed variations: P_r decreases and I_{SPS} increases. Such an effect has already been observed in Ar–SiH_4 discharges, and is interpreted as the appearance of dusts in the plasma. Nanoparticles (few nanometres in diameter) are formed, and induce a variation of the impedance of the plasma, making it become more resistive. The plasma coupling gets closer to its CWC value and P_r decreases (Bélenguer *et al* 1990). As P_i is kept constant, a decrease in P_r means an increase in absorbed RF power. This power excess is dissipated in the discharge, and makes the electric field increase. This induces an increase in T_e and n_e leading to the observed increase in I_{SPS}. The respective contributions of n_e and T_e cannot be deduced from this result, however. On the other hand, during phase 2, $|V_{dc}|$ is practically constant. As $|V_{dc}|$ mainly depends on electron density, this could mean that n_e does not vary much. Consequently, the increase in I_{SPS} might be due essentially to an increase in T_e.

Phase 3 starts when $|V_{dc}|$ begins to decrease, while I_{SPS} and P_r go on increasing and decreasing, respectively. As we said before, a decrease in P_r means an increase in absorbed RF power, and a more efficient coupling (getting closer to CWC conditions). T_e and n_e should then increase. However, the observed decrease in $|V_{dc}|$ indicates that less electrons impact the electrode and globally, n_e decreases. Such an effect has already been observed in Ar–SiH_4 capacitive plasmas (Jouanny 2005), and is interpreted as an electron attachment on the electronegative dusts which have grown in the plasma. The observed increase in I_{SPS} can then only be explained by an increase in T_e. This result confirms the conclusions of section 3.2: when the electrons are less numerous in the plasma, their energy increases. At the end of phase 3, P_r has reached its minimal value, and the coupling is maximal.

Phase 4 starts with an increase in P_r and stops when P_r reaches its maximum. This P_r variation is not understood. It induces a decrease in absorbed RF power, which means the electric field is reduced. As a consequence, I_{SPS} decreases, and so do T_e and n_e. However, during this phase, dusts are still growing, and the electron attachment is still in progress. The decrease in n_e is then due to both the electron attachment onto the dust particles and the decrease in absorbed RF power; and $|V_{dc}|$ decreases faster than in phase 3. However, at the end of phase 4, $|V_{dc}|$ seems to decrease much more slowly. Such behaviour is not well reproducible, and is not understood.

The beginning of phase 5 corresponds to a decrease in P_r. There again, this variation is not understood. It induces an increase in RF absorbed power, and so I_{SPS} increases. At the beginning of this phase, $|V_{dc}|$ is minimal and starts

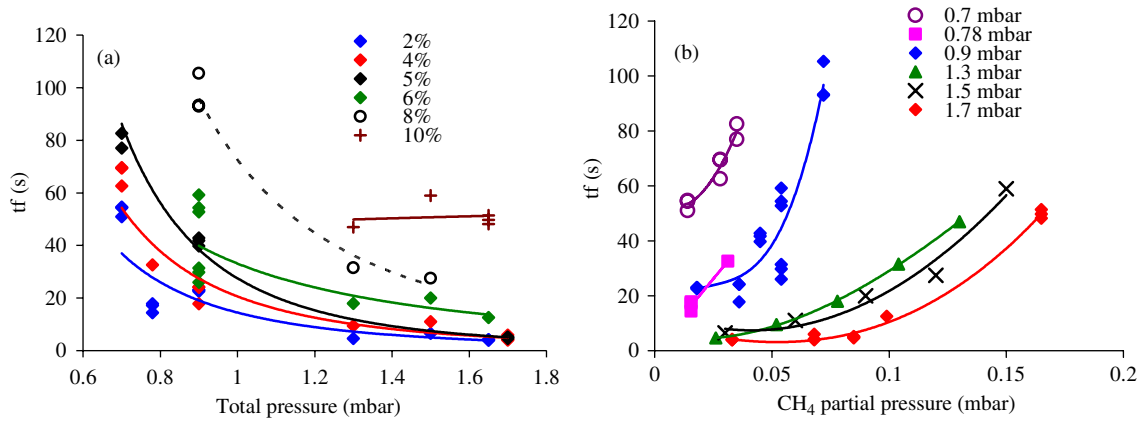


Figure 11. Variations of t_f with total pressure (a) and with the partial pressure of CH_4 (b).

increasing, indicating that the electron density increases. This may correspond to the beginning of dust expulsion out of the confining cage. Note that, at the end of phase 5, $|V_{dc}|$ increases faster, in correlation with a sudden decay of P_r. This behaviour might betray the appearance of a typical instability in capacitive devices, called a 'void' (Jouanny 2005, Cavarroc 2008). When a void is formed, dusts are repelled from the centre of the plasma and stay confined near the cage walls. Up to now, with these results, it has not been possible to decouple the effect of this instability and the expulsion of dust.

Phase 6 corresponds to the section where, at the end of phase 5, all signals stabilize, and no variations are observed until the plasma is switched off. During this phase, particles expelled out of the discharge are replaced by newly formed particles. The electron flow on the electrode is balanced by the electron attachment on dusts: continuous working conditions are reached, and the transient regime is over.

As the formation time of the nanoparticles (end of phase 1) is not clearly measurable for all the studied conditions, we considered the time when $|V_{dc}|$ starts decreasing instead. As we said before, this time, t_f, at the end of phase 2, corresponds to the moment when dusts start agglomerating and thus attaching electrons. It corresponds to the duration of phases 1 and 2, and characterizes the formation kinetics time of dust. We have studied the influence of the pressure and of the amount of CH_4 in the gas mixture on t_f.

The results of this study are presented in figure 11. Figure 11(a) presents the variations of t_f with total pressure for different percentages of CH_4. Figure 11(b) presents the variations of t_f as a function of the CH_4 partial pressure for different total pressures. In both figures, measurements are fitted only to clearly show the main tendencies of t_f variations. The best fits are obtained with a power law curve in figure 11(a), and with a polynomial law curve (order 2 for 1.5 mbar, order 3 for the others) in figure 11(b).

Some of the conditions have been performed several times, to study their reproducibility. At 0.9 mbar, the measurements show a low reproducibility. For example, a factor 2 is observed between t_f measurements at 6% of CH_4 (about 60 and 30 s, see figure 11(a)). On the other hand, as shown in figure 11(b), t_f measurements at high pressure show a good reproducibility. For example, at 1.7 mbar, measured values of t_f are very close for a same condition. It is also interesting to note that data at 1.7 mbar were not all acquired the same day. Indeed t_f was first measured in mixtures containing 2%, 6% and 10% of CH_4. These data were fitted by the curve presented in figure 11(b). About a month later, measurements at 4% and 5% of CH_4 were done. They are perfectly fitted and are in good agreement with previous values.

Figure 11(a) shows that dust particles are formed faster for higher total pressures. This phenomenon is not well understood: at pressures over 1 mbar, and considering a constant electron density, the electron excitation coefficient is expected to decrease (see figure 8). Dissociation reactions would then be less efficient, when the pressure increases, leading to a slower formation of dust. It is clearly not the case. However, due to the great uncertainties on the electron density measurements at such pressures (close to the resolution limit), no strong interpretation can be done by considering the electron energy. On the other hand, as mentioned in section 3.2.1, an increase in pressure leads to an increase in neutral gas temperature and then a variation in chemical kinetics (considering chemical reactions in the gas phase are ruled by Arrhenius laws) leading to a faster formation of dusts. For a more complete explanation, a chemical study of the plasma is needed.

Looking at figure 11(a), it can be assumed that t_f is longer when a larger amount of CH_4 is injected in the discharge. To study this effect, a more relevant parameter is the CH_4 partial pressure which gives the real amount of CH_4 in the discharge. Figure 11(b) confirms this result: the more CH_4 is abundant in the discharge, the longer it takes for dusts to appear. Such a phenomenon has already been observed in a similar discharge but with a different diagnosis by Pereira *et al*: by measuring the intensity of a laser beam scattered by dust in a CCP N_2–CH_4 discharge, they showed that dusts are formed faster when the amount of CH_4 decreases (from 90 to 10%, Pereira *et al* 2008). This effect could be due to the fact that the neutral gas temperature decreases when the amount of CH_4 increases (see figure 6), inducing chemical kinetics decay.

To further explain the dust formation, a chemical study of the plasma, and more precisely of the molecules presumed to be the precursors of the dust formation (Pintassilgo *et al*

1999), such as HCN for example, is necessary. This work is in progress.

5. Conclusion

We have studied an RF CCP discharge, generated at low pressures in different N_2–CH_4 gas mixtures, that simulates Titan's photochemistry, and particularly the formation of solid particles presumed to be analogues of Titan's aerosols. The electron and ion densities were measured, in steady-state dusty plasma conditions. The electron density decreases with pressure for pressures higher than 0.5 mbar, both in pure N_2 and in N_2–CH_4 discharges. We have also shown that the electron density strongly decreases when CH_4 is present in the discharge, even in small proportion. From OES measurements, we have observed that in this CCP discharge, the neutral gas temperature remains close to the ambient temperature. Heating is weak even for an injected power of 100 W, and the neutral gas temperature is decreasing when the amount of CH_4 in the discharge is increased. This variation could have an influence on the kinetics of the solid particles formation.

OES has also allowed us to show some of the changes that occur in the plasma when going from a pure N_2 to a N_2–CH_4 mixture. We have observed that the pressures for a maximal intensity of SPS N_2 bands are strongly modified when CH_4 is injected. Consequently, in pure N_2 discharges, pooling reactions involving $N_2(A)$ metastable state seem to be the main population process for the $N_2(C)$ state. However, this process is probably inefficient in N_2–CH_4 mixtures. This shows a possible strong quenching of $N_2(A)$ when CH_4 is present.

We have estimated the evolution of the electron energy using Ar as an actinometer. Whereas the presence of CH_4 molecules in the gas phase reduces the electron density, it seems to increase the electron energy. This shows that a decay of the electrons' density in the discharge can be compensated by an increase in their energy.

From the study of the plasma in pulsed mode, we have shown that the variations of the self-bias voltage and the OES intensities are correlated. They can be separated in two phases corresponding to the formation of the dusts and their growth. The dust formation is a slow process taking from 4 to 110 s depending on the experimental conditions. The dust formation is faster at high pressure and when the amount of CH_4 in the gas mixture is small. The variations in the time formation of dust do not seem to be correlated with changes in the plasma parameters. A further interpretation might be provided by a study of the chemical kinetics. Moreover, a modelling of the RF discharge in N_2–CH_4 mixtures is necessary to understand the evolution of the plasma parameters. This work is in progress.

Acknowledgments

This work was supported by the French network 'Plasmas Froids', and the Programme National de Planétologie of the CNRS.

References

Allen J E 1995 Probe theories and applications: modern aspects *Plasma Sources Sci. Technol.* **4** 234–41

Bélenguer P and Boeuf J P 1990 Transition between different regimes of rf glow discharges *Phys. Rev.* A **41** 8

Bernard J M, Coll P, Coustenis A and Raulin F 2003 Experimental simulation of Titan's atmosphere: detection of ammonia and ethylene oxide *Planet. Space Sci.* **51** 1003–11

Bogaerts A 2002 Gas discharge plasmas and their application *Spectrochim. Acta* B **57** 609

Bouchoule A and Boufendi L 1993 Particulate formation and dusty plasma behaviour in argon–silane RF discharge *Plasma Sources Sci. Technol.* **2** 204–13

Bouchoule A 1999 *Dusty Plasmas: Physics, Chemistry and Technological Impacts in Plasma Processing* (New York: Wiley)

Boufendi L and Bouchoule A 1994 Particle nucleation and growth in a low-pressure argon–silane discharge *Plasma Sources Sci. Technol.* **3** 262–67

Cavarroc M 2007 Nucléation, croissance et comportement de poussières dans les plasmas réactifs radiofréquences basse pression: des nanocristaux aux grains submicroniques polycristallins *PhD Thesis* University of Orleans, France

Cavarroc M, Mikikian M, Perrier G and Boufendi L 2006 Single-crystal silicon nanoparticles: an instability to check their synthesis *Appl. Phys. Lett.* **89** 013107

Cavarroc M, Mikikian M, Tessier Y and Boufendi L 2008 Successive generations of dust in complex plasmas: a cyclic phenomenon in the void region *Phys. Rev. Lett.* **100** 045001

Coll P, Coscia D, Smith D, Gazeau M C, Ramirez S I, Cernogora G, Israel G and Raulin F 1999 Experimental laboratory simulation of Titan's atmosphere: aerosols and gas phase *Planet. Space Sci.* **47** 1331–40

De Vanssay E, Gazeau M C, Guillemein J C and Raulin F 1995 Experimental simulation of Titan's organic chemistry at low temperature *Planet. Space Sci.* **43** 25–31

Donovan S, Klein O, Dressel M, Holczer K and Grüner G 1993 Microwave cavity perturbation technique: II. Experimental scheme *Int. J. Infrared Millim. Waves* **14** 2459–87

Draine B T and Sutin B 1987 Collisional charging of interstellar grains *Astrophys. J.* **320** 803–17

Dressel M, Klein O, Donovan S and Grüner G 1993 Microwave cavity perturbation technique: III. Applications *Int. J. Infrared Millim. Waves* **14** 2489–517

Géraud-Grenier I, Massereau-Guilbaud and Plain A 2004 Characterization of particulates and coatings created in a 13.56 MHz radiofrequency methane plasma *Surf. Coat. Technol.* **187** 336–42

Hargis P J *et al* 1994 The gaseous electronic conference radio frequency reference cell: a defined parallel plate radio frequency system for experimental and theoretical studies of plasma processing discharges *Rev. Sci. Instrum.* **65** 140–54

Haverlag M, Kroesen G M W, Bisschops T H J and De Hoog F J 1991 Measurement of electron densities by a microwave cavity method in 13.56-MHz RF plasmas of Ar, CF_4, C_2F_6, and CHF_3 *Plasma Chem. Plasma Process.* **11** 357–70

Hong S, Berndt J and Winter J 2003 Growth precursors and dynamics of dust particle formation in the Ar/CH_4 and Ar/C_2H_2 plasmas *Plasma Sources Sci. Technol.* **12** 46–52

Imanaka H, Khare B N, Elsila J E, Bakes E L O, Mc Kay C P, Cruikshank D P, Sugita S, Matsui T and Zare R N 2004 Laboratory experiment of Titan tholins formed in cold plasma at various pressures: implications for nitrogen-containing polycyclic aromatic compounds in Titan haze *Icarus* **168** 344–66

Israel G *et al* 2005 Complex organic matter in Titan's atmospheric aerosols from *in situ* pyrolisis and analysis *Nature* **438** 796–99

Iwai T, Savadatti M I and Broida H P 1967 Mechanisms of populating electronically excitated CN in active nitrogen flames *J. Chem. Phys.* **47** 3861–74

Jenq J J, Ding J, Taylor J W and Hershkowitiz N 1994 Absolute fluorine atom concentrations by RIE and ECR CF4 plasmas measured by actinometry *Plasma Sources Sci. Technol.* **3** 154–61

Jouanny M C 2005 Etude et contrôle de la phase initiale de formation de poudres nanométriques dans les plasmas froids, basse pression en dilution argon–silane et hydrogène–silane *PhD Thesis* University of Orleans, France

Klein O, Donovan S, Dressel M and Grüner G 1993 Microwave cavity perturbation technique: I. Principles *Int. J. Infrared Millim. Waves* **14** 2423–57

Kovacevic E, Stefanovic I, Berndt J and Winter J 2003 Infrared fingerprints and periodic formation of nanoparticles in Ar/C_2H_2 plasmas *J. Appl. Phys.* **93** 2924–30

Lee Y H and Chen M M 1983 Silicon etching mechanism and anisotropy in CF_4+ O_2 plasma *J. Appl. Phys.* **54** 5966–73

Macko P, Veis P and Cernogora G 2004 Study of oxygen atom recombination on a Pyrex surface at different wall temperatures by means of time-resolved actinometry in a double pulse discharge technique *Plasma Sources Sci. Technol.* **13** 251–62

Majumdar A, Behnke J F, Hippler H, Matyash K and Schneider R 2005 Chemical reactions studies in CH_4/Ar and C_2H_2/N_2 mixtures of a dielectric barrier discharge *J. Chem. Phys.* A **109** 9371–7

Marques L, Pintassilgo C D, Alcouffe G, Cernogora G and Alves L 2008 Modeling of nitrogen CCRF discharges used to study Titan's atmosphere *Europhys. Conf. on the Atomic and Molecular Physics of Ionized Gases (Granada, Spain, 15–19 July 2008)*

Marques L, Pintassilgo C D, Alcouffe G, Alves L L and Cernogora G 2008a AIPCP1041 Multifacets of dusty plasmas *Fifth Int. Conf. on the Physics of Dusty Plasma*

Marques L, Pintassilgo C D, Alcouffe G, Cernogora G and Alves L L 2008b Modeling of nitrogen CCRF discharges used to study Titan's atmosphere *19th European Conf. on the Atomic and Molar Physics of Ionized Gases*

Massereau-Guilbaud M, Géraud-Grenier I and Plain A 2000 Influence of particulates generated in a CH_4 low pressure radiofrequency discharge on dc negative self bias voltage *Eur. Phys. J. Appl. Phys.* **11** 71–6

Mikikian M and Boufendi L 2004 Experimental investigations of void dynamics in a dusty discharge *Phys. Plasmas* **11** 3733–7

Navarro-Gonzalez R, Ramirez S I, De La Rosa J G, Coll P and Raulin F 2001 Production of hydrocarbons and nitriles by electric processes in Titan's atmosphere *Adv. Space Res.* **27** 271–82

Papoular R and Balazard J 1991 *Application des Ondes Hyperfréquences et Infrarouge à l'étude des Plasmas* (Paris: Dunod)

Pearse R W B and Gaydon A G 1976 *The Identification of Molecular Spectra* (London: Chapman and Hall)

Pereira J, Géraud-Grenier I, Masserau-Guilbaud V, Plain A and Fernandez V 2006 Characterization of a CN_x : H particles and coatings prepared in a CH_4/N_2 r.f. plasma *Surf. Coat. Technol.* **200** 6414–9

Pereira J, Massereau-Guilbaud V, Géraud-Grenier I and Plain A 2008 Nitrogen effect on the dust presence and behaviour in a radio frequency CH_4/N_2 discharge *J. Appl. Phys.* **103** 033301

Pintassilgo C D, Loureiro J, Cernogora G and Touzeau M 1999 Methane decomposition and active nitrogen in a N_2-CH_4 glow discharge at low pressures *Plasma Sources Sci. Technol.* **8** 463–78

Piper L G 1988 State-to-state $N_2(A\,^3\Sigma_u^+)$ energy-pooling reactions: I. The formation of $N_2(C\,^3\Pi_u)$ and the Herman infrared system *J. Chem. Phys.* **88** 231–9

Praburam G and Goree J 1996 Experimental observation of very low-frequency macroscopic modes in a dusty plasma *Phys. Plasmas* **3** 1212

Provencher G M and McKenney D J 1971 CN emission in active nitrogen: II. The role of energy transfer and atom transfer reactions in $CN(X\,^2\Sigma^+)$ excitation *Can. J. Chem.* **50** 2527–36

Ramirez S I, Navarro–Gonzaelez R, Coll P and Raulin F 2005 Organic chemistry induced by corona discharges in Titan's troposphere: laboratory simulations *Adv. Space Res.* **36** 274–80

Samsonov D and Goree J 1999 Instabilities in a dusty plasma with ion drag and ionization *Phys. Rev.* E **59** 1047–58

Selwyn G S, Singh J and Bennett R S 1989 In situ laser diagnostics studies of plasma-generated particulate contamination *J. Vac. Sci. Technol.* A **7** 2758–64

Slanger T G, Wood B J and Black G 1973 Temperature-dependent $N_2(A\,^3\Sigma_u^+)$ quenching rate coefficients *J. Photochem.* **2** 63

Slater J C 1946 Microwave electronics *Rev. Mod. Phys.* **18** 441

Spears K G, Robinson J T and Roth R M 1986 Particle distribution and laser–particle interactions in an RF discharge of silane *IEEE Trans. Plasma Sci.* **14** 179–87

Spears K G, Kampf R P and Robinson J T 1988 Particle densities in radio-frequencies discharges of silane *J. Phys Chem.* **92** 5297

Szopa C, Cernogora G, Boufendi L, Correia J J and Coll P 2006 PAMPRE: A dusty plasma experiment for Titan's tholins production and study *Planet. Space Sci.* **54** 394–404

Tomasko M G *et al* 2005 Rain, winds and haze during the Huygens probe's descent to Titan's surface *Nature* **438** 765–78

Washida N, Kley D, Becker K H and Groth W 1975 Experimental study of the $C(^3P)+N(^4S)+M \rightarrow CN(B\,^2\Sigma^+)+M$ recombination *J. Chem. Phys.* **63** 4230–41

Watanabe Y, Shiratani M, Kubo Y, Ogawa I and Ogi S 1988 Effects of low-frequency modulation on rf discharge chemical vapour deposition *Appl. Phys. Lett.* **53** 1263–5

NIST Atomic spectra database http://physics.nist.gov/cgi-bin/ASD/lines1.pl